ChemistryOpen

Research Article
doi.org/10.1002/open.202200263

Chemistry Europe
European Chemical Societies Publishing

www.chemistryopen.org

Contradicting Influence of Zn Alloying on Electronic and Thermal Properties of a YbCd$_2$Sb$_2$-Based Zintl Phase at 700 K

Seung-Hwan Kwon[+],[a] Sang-il Kim[+],[a] Weon Ho Shin[+],[b] Seong-Mee Hwang,[a] Kiyoung Lee,[c] Won-Seon Seo,[d] and Hyun-Sik Kim*[a]

Zintl compounds are promising thermoelectric materials for power generation as their electronic and thermal transport properties can be simultaneously engineered with anion/cation alloying. Recently, a peak thermoelectric figure-of-merit, zT, of 1.4 was achieved in a (Yb$_{0.9}$Mg$_{0.1}$)Cd$_{1.2}$Mg$_{0.4}$Zn$_{0.4}$Sb$_2$ Zintl phase at 700 K. Although the effects of alloying Zn in lattice thermal conductivity had been studied thoroughly, how the Zn alloying affects its electronic transport properties has not yet been fully investigated. This study evaluates how the Zn alloying at Cd sites alters the band parameters of (Yb$_{0.9}$Mg$_{0.1}$)Cd$_{1.6-x}$Mg$_{0.4}$Zn$_x$Sb$_2$ ($x = 0$-0.6) using the Single Parabolic Band model at 700 K. The Zn alloying increased the density-of-states effective mass (m_d^*)

from 0.87 to 0.97 m_0. Among Zn-alloyed samples, the m_d^* of the $x = 0.4$ sample was the lowest (0.93 m_0). The Zn alloying decreased the non-degenerate mobility (μ_0) from 71 to 57 cm^2 s^{-1} V^{-1}. Regardless of Zn alloying content, the μ_0 of the Zn-alloyed samples were similar (~57 cm^2 s^{-1} V^{-1}). Consequently, the $x = 0.4$ with the highest zT exhibited the lowest weighted mobility (μ_W). The lowest μ_W represents the lowest theoretical electronic transport properties among other x. The highest zT at $x = 0.4$ despite the lowest μ_W was explained with a significant lattice thermal conductivity reduction achieved with Zn alloying with $x = 0.4$, which outweighed the deteriorated electronic transport properties also due to the alloying.

Introduction

Green energy harvesting, which converts ambient energy into electrical power without consuming fossil fuels, is a sustainable technology.[1] Among the sustainable technologies, thermoelectric technology directly converts thermal energy into electricity. This thermal-to-electrical energy conversion can be explained by the Seebeck effect, which refers to the electric potential induced by the movement of electrons/holes due to temperature gradient.[2] However, the commercial application of thermoelectric devices is limited, mainly because of the low conversion efficiency of the material adopted in the devices.[3] The

conversion efficiency of thermoelectric materials is determined by the figure-of-merit, $zT = S^2 \sigma T / (\kappa_e + \kappa_l)$, where S is the Seebeck coefficient, σ is the electrical conductivity, T is the absolute temperature, κ_e is the electronic thermal conductivity, and κ_l is the lattice thermal conductivity.[1] The performance of thermoelectric materials can be improved by either enhancing the $S^2\sigma$, the power factor (PF), or reducing the κ_l.[4] However, due to the trade-off relationship between the S and σ with varying carrier concentrations, the PF improvement is not straightforward. In contrast, the reduction in κ_l, independent from other thermoelectric parameters, always guarantees the zT enhancement.

Zintl compounds have been studied intensively as promising candidate materials for thermoelectric energy harvesting due to their intrinsically low κ_l originating from complex crystal structures, and excellent σ stemming from the delocalized valence electrons.[5] Therefore, they are often referred to as an ideal example of the phonon-glass electron-crystal (PGEC) concept. Several different types of Zintl compounds like XY_2Sb$_2$,[6,7] $X_{14}Y$Sb$_{11}$,[8,9] $X_9Y_{4.5}$Sb$_2$,[10,11] and X_5Z_2Sb$_6$ ($X =$ Ca, Sr, and Eu, Yb; $Y =$ Cd, Zn, and Mn; $Z =$ Al, Ga, and In) have been reported to display high thermoelectric performance.[12,13] Anions in the Zintl compound are responsible for electronic transport properties, while cations act as phonon-scattering centers.[14] In other words, electronic and thermal conductions can be engineered simultaneously by simple composition tuning.

Recently, Feng et al. achieved a high zT of ~1.0 at 673 K in porous YbCd$_2$Sb$_2$, which is XY_2Sb$_2$-type Zintl compound with $X =$ Yb and $Y =$ Cd.[15] The submicron-sized pores with different morphologies introduced in the samples greatly reduced its κ_l while improving the zT. Zhang et al. obtained an excellent zT

[a] S.-H. Kwon,[+] Prof. Dr. S.-i. Kim,[+] S.-M. Hwang, Prof. Dr. H.-S. Kim
Department of Materials Science and Engineering
University of Seoul
02504 Seoul (Republic of Korea)
E-mail: hyunsik.kim@uos.ac.kr

[b] Prof. Dr. W. H. Shin[+]
Department of Electronic Materials Engineering
Kwangwoon University
01897 Seoul (Republic of Korea)

[c] Prof. Dr. K. Lee
Department of Materials Science & Engineering
Hongik University
04066 Seoul (Republic of Korea)

[d] Dr. W.-S. Seo
Department of Materials Science & Engineering
Yonsei University
03722 Seoul (Republic of Korea)

[+] These authors contributed equally to this work

ChemistryOpen

Research Article
doi.org/10.1002/open.202200263

**Chemistry
Europe**
European Chemical
Societies Publishing

(1.4 at 700 K) in $(Yb_{0.9}Mg_{0.1})Cd_{1.2}Mg_{0.4}Zn_{0.4}Sb_2$.[16] They explained that the reported high zT was due to the severe lattice distortion (ultra-low κ_l) induced by the substitutional incorporation of Mg (at Yb and Cd sites) and Zn (at Cd sites) into $YbCd_2Sb_2$. The work by Zhang et al. is important because the κ_l suppressed by alloying was even greater than that obtained by introducing a significant number of pores in the sample. However, the effects of alloying on electronic transport properties have not been investigated in detail. In this study, we estimated band parameters such as the non-degenerate mobility (μ_0), density-of-states (DOS) effective mass (m_d^*),[17] weighted mobility (μ_W),[2] and quality factor (B) by fitting the Single Parabolic Band (SPB) model to the experimental electronic transport properties of $(Yb_{0.9}Mg_{0.1})Cd_{1.6-x}Mg_{0.4}Zn_xSb_2$ ($x=0$–0.6) reported by Zhang et al. at 700 K.[16] For different Zn alloying content, changes in the electronic band parameters were carefully evaluated. It was found that the $(Yb_{0.9}Mg_{0.1})Cd_{1.2}Mg_{0.4}Zn_{0.4}Sb_2$ sample ($x=0.4$) with the highest zT, had the lowest μ_W, which was directly proportional to the theoretical peak PF at optimum carrier concentration. In other words, the Zn alloying beneficial to suppressing κ_l deteriorates the PF in the meantime. Because the κ_l suppression by Zn alloying is significant, its negative effect on PF is difficult to characterize. However, the electronic band parameters analyzed by the SPB model reveal this clearly for the first time. Furthermore, our analysis suggests that careful design of alloying atom and alloying is essential to improve the zT of XY_2Sb_2-type Zintl compounds by enhancing their electronic transport properties (related to μ_W) while maintaining the substantially low κ_l.

Results and Discussion

The m_d^* and μ_0 of $(Yb_{0.9}Mg_{0.1})Cd_{1.6-x}Mg_{0.4}Zn_xSb_2$ ($x=0$, 0.2, 0.4, and 0.6) were estimated from experimental Hall carrier concentration (n_H)-dependent S and Hall mobility (μ_H) at 700 K, respectively, using the SPB model.[18] The acoustic phonon scattering was assumed to be the dominant carrier scattering mechanism. Figure 1(a) presents the measured (symbols) and calculated (lines) S in terms of n_H for varying Zn alloying contents (x). The measured S in terms of n_H was extracted from Zhang et al.[16] According to the SPB model, the S and n_H are defined as below:

$$S = \frac{k_B}{e}\left(\eta - \frac{2F_1(\eta)}{F_0(\eta)}\right) \quad (1)$$

$$n_H = \frac{16\pi}{3}\left(\frac{2m_d^* k_B T}{h^2}\right)^{3/2}\frac{(F_0(\eta))^2}{F_{-1/2}(\eta)} \quad (2)$$

The η, e, k_B, and $F_n(\eta)$ in Equations (1,2) are the reduced electrochemical potential, electric charge, Boltzmann constant, and the Fermi integral of order n, respectively. The $F_n(\eta)$ is, in turn, defined as in Equation (3):
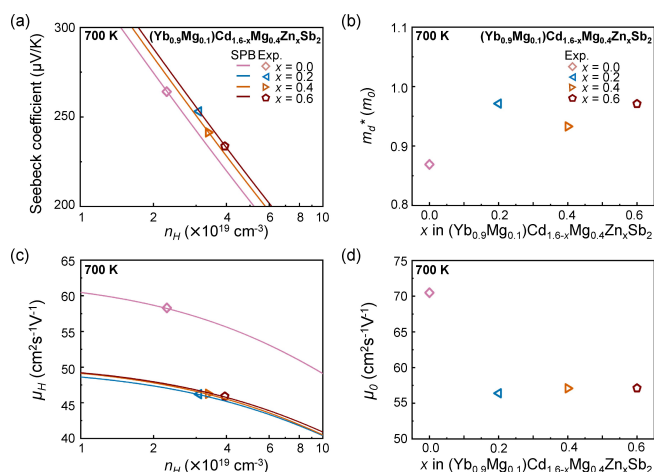

Figure 1. (a) Measured (symbols),[16] and calculated (lines) Seebeck coefficient (S) with varying Hall carrier concentration (n_H) at 700 K. (b) Density-of-states (DOS) effective mass (m_d^*) with varying Zn alloying content (x). (c) Measured (symbols),[15] and calculated (lines) Hall mobility (μ_H) with varying n_H at 700 K. (d) Non-degenerate mobility (μ_0) with varying x.

$$F_n(\eta) = \int_0^\infty \frac{\varepsilon^n}{1+\exp(\varepsilon-\eta)}d\varepsilon \quad (3)$$

The S with varying n_H (in lines) were computed from fitting m_d^* in Equation (2) so that the calculated S with varying n_H (in lines) agreed with the measured data at 700 K. We estimated the band parameters for 700 K because the thermoelectric performance of $(Yb_{0.9}Mg_{0.1})Cd_{1.6-x}Mg_{0.4}Zn_xSb_2$ ($x=0$–0.6) Zintl alloys peaked at 700 K. Experimentally, when the x was increased, the S decreased with an increasing n_H.

Figure 1(b) presents the x-dependent m_d^* at 700 K obtained from Figure 1(a). In general, the m_d^* increased as x increased. For example, the m_d^* of the sample with $x=0$ is 0.87 m_0, the lowest among all the samples. For $x=0.2$ and 0.6, their m_d^* are as high as 0.97 m_0. The average m_d^* of all Zn-alloyed samples ($x>0$) is 0.96 m_0, which is approximately 10% heavier than the m_d^* of the sample with $x=0$. Therefore, it is clear that Zn alloying at the Cd site increases m_d^* compared to the $x=0$ sample. However, the difference among m_d^* of Zn-alloyed samples is not significant (m_d^* of $x=0.2$ and 0.6: 0.97 m_0, m_d^* of $x=0.4$: 0.93 m_0).

Figure 1(c) presents the measured (symbols) and calculated (lines) μ_H in terms of n_H for varying x at 700 K. According to the SPB model, the μ_H is expressed as in Equation (4):

$$\mu_H = \mu_0 \frac{F_{-1/2}(\eta)}{2F_0(\eta)} \quad (4)$$

The μ_H in terms of n_H (in lines) in Figure 1(c) were computed from Equation (2) and Equation (4). The μ_0 in Equation (4) was fitted to place the calculated lines on top of the experimental data. Zn alloying significantly decreased the μ_H of the pristine sample. Although increasing the Zn alloying content increased the n_H, corresponding changes in μ_H were negligible. For instance, the μ_H of the pristine sample is 58.3 $cm^2 s^{-1} V^{-1}$, while the average μ_H of all Zn-alloyed samples is 46.1 $cm^2 s^{-1} V^{-1}$. Zn

ChemistryOpen

Research Article
doi.org/10.1002/open.202200263

Chemistry
Europe
European Chemical
Societies Publishing

alloying suppressed the μ_H of the pristine sample by more than 20%.

Figure 1(d) shows μ_0 estimated from Figure 1(c). Similar to what we have observed in μ_H (Figure 1(c)), Zn alloying decreased the μ_0 of the pristine sample drastically. While the μ_0 of the pristine sample is 70.5 cm^{2}s^{-1}V^{-1}, the average μ_0 of all Zn-alloyed samples is 56.9 cm^{2}s^{-1}V^{-1}, which is 19% lower than that of the pristine sample. Additionally, the discrepancies in μ_0 among the Zn-alloyed samples are not significant. In conclusion, μ_0 is decreased and saturated with Zn alloying, similar to the trend observed for μ_H. The decrease in μ_0 signifies the reinforcement of the carrier-phonon interaction. Thus, the carrier-phonon interaction increases as a result of Zn alloying, resulting in a decrease in μ_H.

Figure 2(a) presents the Lorenz number (L) with varying n_H extracted from the literature (symbols),[16] and estimated from the SPB model (lines). While Zhang et al. also estimated L, we denoted the L from Zhang et al. as 'experimental' L, for simplicity.[16] We calculated the L using Equation (5) below:

$$L = \left(\frac{k_B}{e}\right)^2 \frac{3F_0(\eta)F_2(\eta) - 4F_1^2(\eta)}{F_0^2(\eta)} \qquad (5)$$

According to Equation (5), L depends only on η.[18] Therefore, the Zn alloying effect on the Fermi level (equivalent to η) can be evaluated. The lowest L among all samples was 1.55×10^{-8} WΩK^{-2} which was observed in (Yb$_{0.9}$Mg$_{0.1}$)Cd$_{1.6}$Mg$_{0.4}$Sb$_2$ ($x=0$). In contrast, the highest L was obtained for (Yb$_{0.9}$Mg$_{0.1}$)Cd$_{1.0}$Mg$_{0.4}$Zn$_{0.6}$Sb$_2$ ($x=0.6$) with $L=1.58\times 10^{-8}$ WΩK^{-2}. From the L of (Yb$_{0.9}$Mg$_{0.1}$)Cd$_{1.0}$Mg$_{0.4}$Zn$_{0.6}$Sb$_2$ ($x=0.6$) being 2% higher than that of (Yb$_{0.9}$Mg$_{0.1}$)Cd$_{1.6}$Mg$_{0.4}$Sb$_2$ ($x=0$), it is inferred that the Fermi level is shifted slightly towards the valence band when the x increases. In terms of η, the L of the sample with $x=0$ corresponds to -0.89, which is the lowest η among all samples. Because $\eta=0$ is when the Fermi level is at the top of the valence band (for p-type), $\eta=-0.89$ of the $x=0$ sample corresponds to the situation where theFermi level is
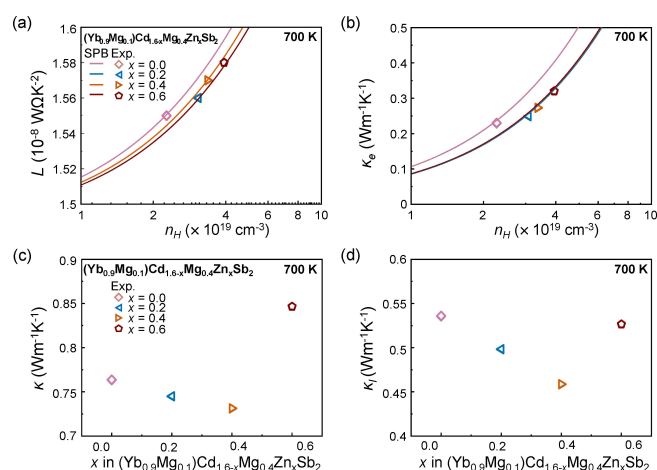
above the top of the valence band. The η for (Yb$_{0.9}$Mg$_{0.1}$)CdMg$_{0.4}$Zn$_{0.6}$Sb$_2$ ($x=0.6$) is -0.45, much closer to the valence band than the $x=0$ is, but still outside of the valence band. The Fermi level outside of the valence band approaches the valence band with Zn alloying at Cd sites. Correspondingly, L increases with an increase in x.

It is observed that Zn alloying significantly increases n_H at 700 K. The n_H of pristine (Yb$_{0.9}$Mg$_{0.1}$)Cd$_{1.6}$Mg$_{0.4}$Sb$_2$ ($x=0$) is 2.27×10^{19} cm^{-3}, the lowest among those of all samples. Conversely, (Yb$_{0.9}$Mg$_{0.1}$)CdMg$_{0.4}$Zn$_{0.6}$Sb$_2$ ($x=0.6$) exhibits an n_H of 3.94×10^{19} cm^{-3}, which is 74% higher than that of the pristine sample. The changes in η and m_d^* with Zn alloying affect the trend of n_H, as corroborated by Equation (2). As mentioned before, m_d^* does not change distinctly with Zn alloying, whereas η increases steadily with increasing Zn alloying content. Consequently, the drastic n_H increase with alloying can be attributed to the η increase.

Figure 2(b) presents the κ_e with varying n_H. Experimental data extracted from the literature are presented in symbols.[16] Equation (6) was employed to obtain the lines shown in Figure 2(b):

$$\kappa_e = L\sigma T \qquad (6)$$

For the calculation of κ_e, the L shown in Figure 2(a) and the σ obtained from Equation (7) were used:

$$\sigma = n_H e \mu_H \qquad (7)$$

In Equation (7), the n_H and μ_H were obtained using Equation (2) and (4), respectively (Figure 1(c)). Equation (7) indicates that σ depends on both μ_H and n_H. As described above, Zn alloying first decreases the μ_H, but no further reduction in μ_H was observed as x increases. At the same time, a significant increase in n_H with Zn alloying is observed with an increasing x. Because the increase in n_H outweighs the decrease in μ_H with varying x, a σ increase with x is expected, and consequently the increase in κ_e. In Figure 2(b), the lowest experimental κ_e is 0.23 W m^{-1} K^{-1}, for the pristine (Yb$_{0.9}$Mg$_{0.1}$)Cd$_{1.6}$Mg$_{0.4}$Sb$_2$ ($x=0$). The highest κ_e is 0.32 W m^{-1} K^{-1}, for (Yb$_{0.9}$Mg$_{0.1}$)Cd$_{1.0}$Mg$_{0.4}$Zn$_{0.6}$Sb$_2$ ($x=0.6$), which is 39% greater than the κ_e of the sample with $x=0$. In addition, κ_e increases steadily with x. Again, the reason behind the observed κ_e trend can be found from Equation (7). Because the temperature is fixed at 700 K in this analysis, it is clear that only L and σ are directly proportional to κ_e. As it is shown in Figure 2(a), the L is increased with Zn alloying, and the σ increase is also expected with the alloying. Therefore, the κ_e increases consistently because both L and σ increase with Zn alloying.

The experimental total thermal conductivity (κ), reported by Zhang et al., is shown in Figure 2(c).[16] As the alloying increases, the κ decreases until $x=0.4$; however, it rapidly increases at alloying content of $x=0.6$ (0.84 W m^{-1} K^{-1}), which is 13% higher than the average κ of rest of the samples ($0\leq x\leq 0.4$). To understand the abrupt increase in κ at $x=0.6$, the κ_e from Figure 2(b) is subtracted from the κ to obtain the κ_l [Eq. (8)]:

Figure 2. Measured (symbols),[16] and calculated (a) Lorenz number (L) and (b) electronic thermal conductivity (κ_e) with varying n_H at 700 K. Experimental (symbols) (c) total thermal conductivity (κ) and (d) lattice thermal conductivity (κ_l) as a function of x.[16]

ChemistryOpen

Research Article
doi.org/10.1002/open.202200263

Chemistry Europe
European Chemical
Societies Publishing

$$\kappa_l = \kappa - \kappa_e \tag{8}$$

κ_l estimated using the calculated κ_e (Figure 2(b)) is presented in Figure 2(d). As shown in Figure 2(d), the κ_l of all Zn-alloyed samples are lower than that of the pristine sample. The κ_l of the pristine sample (0.53 W m^{-1}K^{-1}) is the highest among all the samples. The distinctive reduction in κ_l with alloying is mainly due to the incorporation of substitutional impurities, which increases the point defect phonon scattering.[19,20] Furthermore, the lowest κ_l is obtained for $(Yb_{0.9}Mg_{0.1})Cd_{1.2}Mg_{0.4}Zn_{0.4}Sb_2$ ($x=0.4$) with 0.47 W m^{-1}K^{-1}. The κ_l difference of 11% is observed between the pristine and the $x=0.4$ samples. Primarily, the discrepancies in atomic mass and ionic size between the lattice and alloying atoms are responsible for the strong phonon scattering. The lattice atom (Cd sites) has an atomic mass of 112.41 amu with an ionic size of 158 pm.[21] Meanwhile, the atomic mass and ionic size of the alloying atom (Zn) are 65.38 amu and 139 pm, respectively.[21] The alloying atom (Zn) has an atomic mass and ionic size that are 42% lighter and 12% smaller than those of the Cd sites, respectively. This gap plays a pivotal role in reducing the κ_l. However, the κ_l of $(Yb_{0.9}Mg_{0.1})Cd_{1.0}Mg_{0.4}Zn_{0.6}Sb_2$ ($x=0.6$) increases to 0.52 W m^{-1}K^{-1}, which is higher than those of $(Yb_{0.9}Mg_{0.1})Cd_{1.4}Mg_{0.4}Zn_{0.2}Sb_2$ ($x=0.2$) and $(Yb_{0.9}Mg_{0.1})Cd_{1.2}Mg_{0.4}Zn_{0.4}Sb_2$ ($x=0.4$). This irregularity in κ_l requires further investigation.[22]

The weighted mobility (μ_W) of $(Yb_{0.9}Mg_{0.1})Cd_{1.6-x}Mg_{0.4}Zn_xSb_2$ ($x=0, 0.2, 0.4$, and 0.6) at 700 K, calculated using Equation (9), is shown in Figure 3(a) along with x.

$$\mu_W = \mu_0 \left(\frac{m_d^*}{m_0}\right)^{3/2} \tag{9}$$

A sample with higher m_d^* and μ_0 will have a higher μ_W. Because the m_d^* is related to S and μ_0 to μ_H, the μ_W summarizes the potential PF of the sample. Among all samples, the lowest μ_W is observed for $(Yb_{0.9}Mg_{0.1})Cd_{1.2}Mg_{0.4}Zn_{0.4}Sb_2$ ($x=0.4$) (51.4 cm^{2}s^{-1}V^{-1}). On the contrary, the highest μ_W is 57.1 cm^{2}s^{-1}V^{-1} for the pristine $(Yb_{0.9}Mg_{0.1})Cd_{1.6}Mg_{0.4}Sb_2$ ($x=0$). Accordingly, μ_W of the pristine sample is 11% greater than that of the $x=0.4$ sample, which shows that Zn alloying has a negative impact on μ_W. This decline can mainly be attributed to the decrease in μ_0 after doping. However, the μ_W of $(Yb_{0.9}Mg_{0.1})Cd_{1.0}Mg_{0.4}Zn_{0.6}Sb_2$ ($x=0.6$) (54.6 cm^{2}s^{-1}V^{-1}), which is

6% higher than that of $(Yb_{0.9}Mg_{0.1})Cd_{1.2}Mg_{0.4}Zn_{0.4}Sb_2$ ($x=0.4$), does not follow the trend described above. Such irregularities are corroborated in relation to m_d^* and μ_0. $(Yb_{0.9}Mg_{0.1})Cd_{1.0}Mg_{0.4}Zn_{0.6}Sb_2$ ($x=0.6$) has the highest m_d^* among all the samples, while μ_0 is saturated with Zn doping. Consequently, it can be concluded that the high m_d^* of $(Yb_{0.9}Mg_{0.1})Cd_{1.0}Mg_{0.4}Zn_{0.6}Sb_2$ ($x=0.6$) contributes to the highest μ_W among the alloyed samples.

The n_H-dependent PF is presented in Figure 3(b). These lines fitted to the experimental PF (presented as symbols) are obtained by the product of S^2 and σ both calculated using the band parameters. As it is shown in Figure 3(b), the calculated PF and experimental PF results are in reasonable agreement. After Zn alloying, the experimental PF decreases slightly in all cases, except for $(Yb_{0.9}Mg_{0.1})Cd_{1.0}Mg_{0.4}Zn_{0.6}Sb_2$ ($x=0.6$), which has the highest experimental PF (15.8 µW cm^{-1}K^{-2}) among all samples. The theoretical maximum PF can be interpreted using μ_W. The $x=0.6$ sample with the highest μ_W exhibits the highest PF maximum in Figure 3(b). If the n_H is tuned to 10^{20} cm^{-3}, the corresponding PF would improve by 12% ($15.8 \rightarrow 17.7$ µW cm^{-1}K^{-2}).

The calculated quality factor (B) in terms of x in $(Yb_{0.9}Mg_{0.1})Cd_{1.6-x}Mg_{0.4}Zn_xSb_2$ ($x=0, 0.2, 0.4$, and 0.6) is shown in Figure 4(a). The B was computed using Equation (10):

$$B = \left(\frac{k_B}{e}\right)^2 \frac{8\pi e(2m_0 k_B)^{3/2}}{h^3} \frac{\mu_W T^{5/2}}{\kappa_l} \tag{10}$$

As shown in Figure 4(a), B increases steadily and peaks at $(Yb_{0.9}Mg_{0.1})Cd_{1.2}Mg_{0.4}Zn_{0.4}Sb_2$ ($x=0.4$) (1.90). This tendency can be understood using μ_W and κ_l. Equation (10) indicates that the B is affected by κ_l, T, and μ_W. However, because T is fixed at 700 K, only μ_W and κ_l can change the B. While the B is directly proportional to μ_W, it is inversely proportional to κ_l. According to Figure 3, the highest μ_W was obtained for pristine $(Yb_{0.9}Mg_{0.1})Cd_{1.6}Mg_{0.4}Sb_2$ ($x=0$), whereas the lowest μ_W was obtained for $(Yb_{0.9}Mg_{0.1})Cd_{1.2}Mg_{0.4}Zn_{0.4}Sb_2$ ($x=0.4$). On the contrary, pristine $(Yb_{0.9}Mg_{0.1})Cd_{1.6}Mg_{0.4}Sb_2$ ($x=0$) has the highest κ_l, while the lowest κ_l is obtained for $(Yb_{0.9}Mg_{0.1})Cd_{1.2}Mg_{0.4}Zn_{0.4}Sb_2$ ($x=0.4$). Even though it has the lowest μ_W, it is observed that the highest quality factor (0.29) is obtained at $x=0.4$. This can mainly be attributed to the fact that the low μ_W is compensated by an ultralow κ_l.

The zT is presented in Figure 4(b), as a function of n_H. The lines were obtained using the SPB model, while the symbols represent the experimental zT.[16] According to Figure 4(b), the
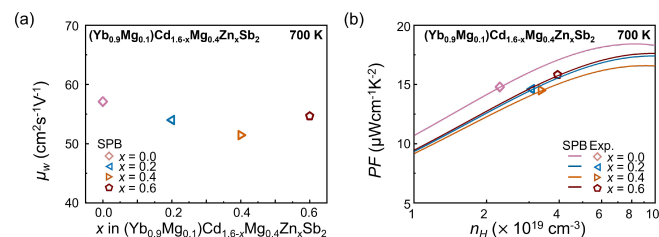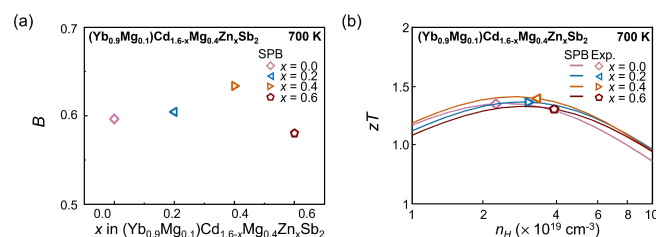

Figure 3. (a) Calculated weighted mobility (μ_W) in terms of x at 700 K. (b) Computed (lines) and measured (symbols) PF in terms of n_H at 700 K.[16]

Figure 4. (a) Calculated quality factor (B) with varying x at 700 K. (b) Computed (lines) and experimental (symbols) zT in terms of n_H at 700 K.[16]

ChemistryOpen

Research Article
doi.org/10.1002/open.202200263

Chemistry Europe
European Chemical
Societies Publishing

zT improves gradually and peaks at $x = 0.4$ (($(Yb_{0.9}Mg_{0.1})Cd_{1.2}Mg_{0.4}Zn_{0.4}Sb_2$), but decreases significantly for $(Yb_{0.9}Mg_{0.1})Cd_{0.6}Mg_{0.4}Zn_{0.6}Sb_2$ ($x = 0.6$). This tendency–both the rise and decline in sequence–is similar to that of B. This similarity can be ascribed to the correlation between B and the peak zT. $(Yb_{0.9}Mg_{0.1})Cd_{1.2}Mg_{0.4}Zn_{0.4}Sb_2$ ($x = 0.4$) has the highest quality factor, whereas the lowest quality factor is observed for $(Yb_{0.9}Mg_{0.1})CdMg_{0.4}Zn_{0.6}Sb_2$ ($x = 0.6$). Accordingly, the highest zT is predicted for $(Yb_{0.9}Mg_{0.1})Cd_{1.2}Mg_{0.4}Zn_{0.4}Sb_2$ ($x = 0.4$) as 1.40. In contrast, the highest zT calculated for $(Yb_{0.9}Mg_{0.1})Cd_{1.0}Mg_{0.4}Zn_{0.6}Sb_2$ ($x = 0.6$) is only 1.31.

Conclusion

In summary, the effects of alloying Zn at Cd sites in $(Yb_{0.9}Mg_{0.1})Cd_{1.6-x}Mg_{0.4}Zn_xSb_2$ ($x = 0$–0.6) have been studied in terms of electronic band parameters. When the Zn alloying content was increased, the corresponding density-of-states effective mass generally increased. On the contrary, the non-degenerate mobility first decreased with Zn alloying, but increasing the alloying content did not further change the non-degenerate mobility. Consequently, the weighted mobility of the $(Yb_{0.9}Mg_{0.1})Cd_{1.2}Mg_{0.4}Zn_{0.4}Sb_2$ ($x = 0.4$) samples was the lowest which meant the lowest theoretical maximum power factor. However, the $x = 0.4$ sample also exhibited the lowest lattice thermal conductivity among all x samples. Hence, the highest zT previously reported for $x = 0.4$ was all because of its ultralow κ_l (0.46 $W\,m^{-1}\,K^{-1}$), since its maximum power factor estimated was lower than those predicted for samples with other x. The fact that a remarkably high zT was attained despite the lowest weighted mobility and power factor highlights the significance of reducing the lattice thermal conductivity through proper doping in improving the performance of thermoelectric materials.

Experimental Section

Using the Single Parabolic Band (SPB) model, the non-degenerate mobility (μ_0) and density-of-states effective mass (m_d^*) were fitted to the experimental electronic transport properties (Seebeck coefficient and Hall mobility) previously reported by Zhang et al.[15] The Lorenz number (L) was also estimated from the SPB model. With the obtained μ_0 and L, the electronic thermal conductivity (κ_e) was calculated. By subtracting the κ_e from the total thermal conductivity measurement,[15] the lattice thermal conductivity (κ_l) was obtained. The weighted mobility (μ_W) was computed with the m_d^* and μ_0. Corresponding power factor as a function of Hall carrier concentration (n_H) was calculated using the SPB model. Finally, the quality factor (B) was computed from μ_W and κ_l. The maximum zT as a function of n_H was also predicted using the B.

Conflict of Interest

The authors declare no conflict of interest.

Data Availability Statement

The data that support the findings of this study are available from the corresponding author upon reasonable request.

[1] B. B. Iversen, *Nat. Mater.* **2021**, *20*, 1309–1310.
[2] M. Kim, S.-i. Kim, S. W. Kim, H.-S. Kim, K. H. Lee, *Adv. Mater.* **2021**, *33*, 2005931.
[3] J. P. Heremans, V. Jovovic, E. S. Toberer, A. Saramat, K. Kurosaki, A. Charoenphakdee, S. Yamanaka, G. J. Snyder, *Science* **2008**, *321*, 554–557.
[4] W. He, D. Wang, H. Wu, Y. Xiao, Y. Zhang, D. He, Y. Feng, Y.-J. Hao, J.-F. Dong, R. Chetty, L. Hao, D. Chen, J. Qin, Q. Yang, X. Li, J.-M. Song, Y. Zhu, W. Xu, C. Niu, X. Li, G. Wang, C. Liu, M. Ohta, S. J. Pennycook, J. He, J.-F. Li, L.-D. Zhao, *Science* **2019**, *365*, 1418–1424.
[5] C. Chen, W. Xue, S. Li, Z. Zhang, X. Li, X. Wang, Y. Liu, J. Sui, X. Liu, F. Cao, Z. Ren, C.-W. Chu, Y. Wang, Q. Zhang, *Proc. Natl. Acad. Sci. USA* **2019**, *116*, 2831–2836.
[6] J. Sun, J. Shuai, Z. Ren, D. J. Singh, *Mater. Today Phys.* **2017**, *2*, 40–45.
[7] X. Wang, W. Li, C. Wang, J. Li, X. Zhang, B. Zhou, Y. Chen, Y. Pei, *J. Mater. Chem. A* **2017**, *5*, 24185–24192.
[8] S. R. Brown, S. M. Kauzlarich, F. Gascoin, G. J. Snyder, *Chem. Mater.* **2006**, *18*, 1873–1877.
[9] A. P. Holm, T. C. Ozawa, S. M. Kauzlarich, S. A. Morton, G. D. Waddill, J. G. Tobin, *J. Solid State Chem.* **2005**, *178*, 262–269.
[10] J. Shuai, J. Mao, S. Song, Q. Zhang, G. Chen, Z. Ren, *Mater. Today Phys.* **2017**, *1*, 74–95.
[11] C. Chen, W. Xue, X. Li, Y. Lan, Z. Zhang, X. Wang, F. Zhang, H. Yao, S. Li, J. Sui, X. Liu, F. Cao, Y. Wang, Q. Zhang, *ACS Appl. Mater. Interfaces* **2019**, *11*, 37741–37747.
[12] Y. L. Yan, Y. X. Wang, G. B. Zhang, *Comput. Mater. Sci.* **2014**, *85*, 88–93.
[13] U. Aydemir, A. Zevalkink, A. Ormeci, H. Wang, S. Ohno, S. Bux, G. J. Snyder, *Dalton Trans.* **2015**, *44*, 6767–6774.
[14] W. Zhang, C. Chen, H. Yao, W. Xue, S. Li, F. Bai, Y. Huang, X. Li, X. Lin, F. Cao, J. Sui, S. Wang, B. Yu, Y. Wang, X. Liu, Q. Zhang, *Chem. Mater.* **2020**, *32*, 6983–6989.
[15] J. Fang, W. Wang, S. Huang, B. Jiang, B. Zhu, Y. Zhu, J. Cui, P. Lin, L. Xie, J. He, *ACS Appl. Energ. Mater.* **2021**, *4*, 913–920.
[16] Z. Zhang, H. Yao, Q. Wang, W. Xue, Y. Wang, L. Yin, X. Wang, X. Li, C. Chen, J. Sui, X. Lin, Y. Chen, X. Liu, J. Mao, G. Xie, Q. Zhang, *Adv. Funct. Mater.* **2022**, *32*, 2205215.
[17] K. H. Lee, S.-i. Kim, J.-C. Lim, J. Y. Cho, H. Yang, H.-S. Kim, *Adv. Funct. Mater.* **2022**, *32*, 2203852.
[18] A. F. May, G. J. Snyder, in *Thermoelectrics and its Energy Harvesting* (Ed. D. M. Rowe), CRC Press, London, England. **2012**, Ch. 1.
[19] Y. Pei, L. Zheng, W. Li, S. Lin, Z. Chen, Y. Wang, X. Xu, H. Yu, Y. Chen, B. Ge, *Adv. Electron. Mater.* **2016**, *2*, 1600019.
[20] H.-S. Kim, S.-i. Kim, K. H. Lee, S. W. Kim, G. J. Snyder, *Phys. Status Solidi B* **2017**, *5*, 1600103.
[21] R. D. Shannon, *Acta Crystallogr. Sect. A* **1976**, *32*, 751–767.
[22] J. Callaway, *Phys. Rev.* **1959**, *113*, 1046–1051.